JACS
JOURNAL OF THE AMERICAN CHEMICAL SOCIETY

Article

pubs.acs.org/JACS

# Proton–Electron Transport and Transfer in Electrocatalytic Films. Application to a Cobalt-Based $O_2$-Evolution Catalyst

D. Kwabena Bediako,[†] Cyrille Costentin,*[,‡] Evan C. Jones,[†] Daniel G. Nocera,*[,†] and Jean-Michel Savéant*[,‡]

[†]Department of Chemistry and Chemical Biology, 12 Oxford Street, Harvard University, Cambridge, Massachusetts 02138-2902, United States

[‡]Sorbonne Paris Cité, Laboratoire d'Electrochimie Moléculaire, Unité Mixte de Recherche Université - CNRS No 7591, Université Paris Diderot, Bâtiment Lavoisier, 15 rue Jean de Baïf, 75205 Paris Cedex 13, France

Supporting Information

**ABSTRACT:** Solar-driven electrochemical transformations of small molecules, such as water splitting and $CO_2$ reduction, pertinent to modern energy challenges, require the assistance of catalysts preferably deposited on conducting or semiconducting surfaces. Understanding mechanisms and identifying the factors that control the functioning of such systems are required for rational catalyst optimization and improved performance. A methodology is proposed, in the framework of rotating disk electrode voltammetry, to analyze the current responses expected in the case of a semigeneral reaction scheme involving a proton-coupled catalytic reaction associated with proton-coupled electron hopping through the film as rate controlling factors in the case where there is no limitation by substrate diffusion. The predictions concern the current density vs overpotential (Tafel) plots and their dependence on buffer concentration (including absence of buffer), film thickness and rotation rate. The Tafel plots may have a variety of slopes (e.g., $F/RT \ln 10$, $F/2RT \ln 10$, 0) that may even coexist within the overpotential range of a single plot. We show that an optimal film thickness exists beyond which the activity of the film plateaus. Application to water oxidation by films of a cobalt-based oxidic catalyst provides a successful test of the applicability of the proposed methodology, which also provides further insight into the mechanism by which these cobalt-based films catalyze the oxidation of water. The exact nature of the kinetic and thermodynamic characteristics that have been derived from the analysis is discussed as well as their use in catalyst benchmarking.

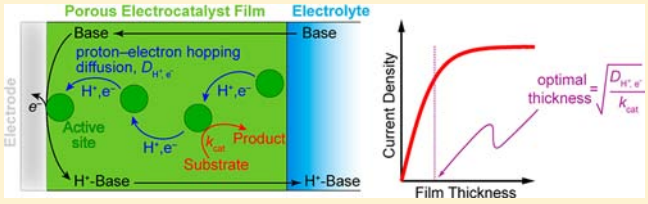


## INTRODUCTION

To meet rising global energy demand, inexpensive and carbon-neutral energy sources must be developed to ensure the sustainable development of future generations.[1] Solar-driven electrochemical splitting of water to molecular hydrogen and oxygen,[2] along with the reduction of carbon dioxide[3] are small molecule transformations that hold promise as routes of storing sunlight in energy-dense chemical bonds. Electrochemical recovery of the stored energy would then involve the oxidation of hydrogen or the $CO_2$-derived fuel in a fuel cell.[4,5]

In most of these cases, high activation penalties require the help of catalysts, usually transition-metal derivatives, which may be operated homogeneously or under the form of a thin film that coats an electrode. The latter arrangement is preferred since it allows compactness and avoids reactant separation problems. Identifying the factors that control the functioning of such devices and understanding their interplay are required for rational catalyst optimization and improved performance. Besides the catalytic reaction itself, two major controlling factors are (i) the transport of electrons from or to the electrode to regenerate the active form of the catalyst and (ii) the transport of the substrate from the bathing solution through the film toward the catalytic centers. In the above-listed reactions and in many others, protons are consumed or produced during catalysis. Proton-coupled electron transfer (PCET) reactions[6] thus play a key role in the catalytic cycle. The transport of protons and/or the acid and basic forms of the buffer often added to the solution may therefore influence the catalytic responses. In such systems, one should consider also that the transport of electrons through the film may be coupled with the transfer of protons. The purpose of the work reported herein was to investigate the interplay of these various, potentially governing factors in the framework of a reasonably general process. A completely general analysis would embark the reader in a taxonomic nightmare with no guarantee of actual generality. In contrast, a reasonably general reaction scheme should retain most of the essential controlling factors, with some simplifying assumptions, allowing a tractable analysis of their interplay. Scheme 1, with some accompanying simplifications and approximations, as detailed in the following study, represents such a reasonably general framework. It is represented for an oxidative process. Transposition to reduction is straightforward. One of the main simplifying assumptions is that the substrate is in large

**Received:** April 23, 2013
**Published:** June 12, 2013

   dx.doi.org/10.1021/ja403656w | J. Am. Chem. Soc. 2013, 135, 10492–10502

**Scheme 1. Electrocatalytic Oxidation of the Substrate A into the Products B in the Presence of an Acid–Base Couple (charge not shown) ZH/Z by Means of an Immobilized PH/Q + e⁻ Catalyst Couple**

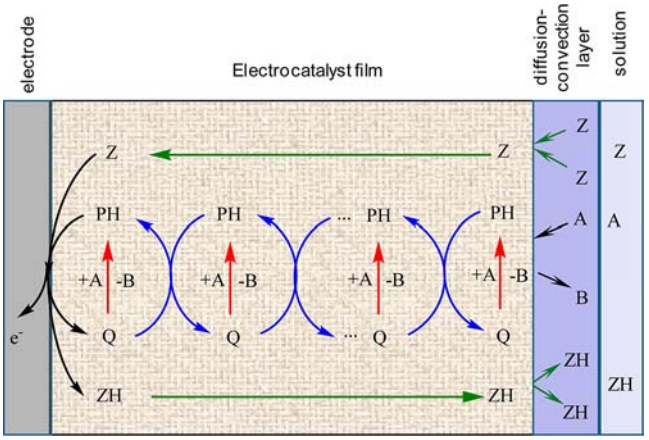


concentration in the solution and in the film, so large that it remains constant as it is the case when the solvent, e.g., water, is the substrate. This simplifying situation is considered in order to focus on the other factors, notably proton transfer and transport. Cases in which penetration and diffusion of the substrate through the film are rate-controlling factors may be treated when necessary by adaptation of the present and previous analyses.[7]

The kinetic responses expected for such processes will be discussed in the first part of this paper, as the result of interplay between the various rate-controlling factors. The second part will be devoted to the application of this methodology to the electrocatalytic oxidation of water by a cobalt oxide film in a family of thin-film oxidic catalysts[8] that have been shown to be promising candidates for direct solar water splitting systems,[9] in large part because of their capacity for self-repair.[10] Self-repair permits their operation under a wide range of pH conditions, including close-to-neutral pHs. Spectroscopic studies[11] of these cobalt-based catalysts (Co–OECs) have established a mixed valence $Co^{III/IV}$ resting state, and mechanistic studies[12] suggest a rapid, one-electron, one-proton equilibrium between $Co^{III}$–OH and $Co^{IV}$–O in which a phosphate species is the proton acceptor, followed by a chemical turnover-limiting process involving oxygen–oxygen bond coupling (Scheme 2). Subsequently, lower valence intermediates are rapidly oxidized to regenerate the resting state species (a net $3e^-$, $3H^+$ process), and thus the kinetics of these steps do not contribute to the overall rate law. As a consequence, the cobalt-based $O_2$-evolution catalyst may be

**Scheme 2. Electrocatalytic Oxidation of Water into the Products Dioxygen and Protons in the Presence of an Acid–Base Couple (charge not shown) ZH/Z (possibly $H_3O^+$/$H_2O$)**

$$\text{4 times}\quad Co^{III}OH\text{-}Co^{IV}O + Z \rightleftharpoons Co^{IV}O\text{-}Co^{IV}O + ZH + e$$

$$Co^{IV}O\text{-}Co^{IV}O + 2\,H_2O \xrightarrow{k_C} Co^{II}OH_2\text{-}Co^{II}OH_2 + O_2$$

$$Co^{IV}O\text{-}Co^{IV}O + Co^{II}OH_2\text{-}Co^{II}OH_2 \xrightarrow{k > k_C} Co^{III}OH\text{-}Co^{IV}O + Co^{III}OH\text{-}Co^{II}OH_2$$

$$Co^{IV}O\text{-}Co^{IV}O + Co^{III}OH\text{-}Co^{II}OH_2 \xrightarrow{k' > k_C} Co^{III}OH\text{-}Co^{IV}O + Co^{III}OH\text{-}Co^{III}OH$$

$$Co^{IV}O\text{-}Co^{IV}O + Co^{III}OH\text{-}Co^{III}OH \xrightarrow{k'' > k_C} 2\,Co^{III}OH\text{-}Co^{IV}O$$

$$2\,H_2O + 4\,Z \longrightarrow O_2 + 4\,ZH + 4\,e$$

analyzed according to a simple scheme (Scheme 1) that involves the PH ($Co^{IV}O$–$Co^{III}OH$) and Q ($Co^{IV}O$–$Co^{IV}O$) forms of the catalyst merely considering that $k_{cat} = 4 \times k_C$ in eqs 2 and 3. As porous materials, the accessibility of active sites distributed throughout the film is a key determinant of overall OER activity.[13]

## RESULTS AND DISCUSSION

**1. Electrocatalytic Oxidation of a Substrate by Means of an Immobilized Proton–Electron Catalyst Couple.** Although any electrochemical nondestructive technique may be used to investigate the kinetic responses of systems like the one shown in Scheme 1, rotating-disk electrode voltammetry (RDEV) is particularly convenient and holds transport characteristics that are similar to those prevailing under preparative-scale conditions. Transport of the reactants in the solution to or from the film/solution may be controlled through the rotating rate, $\omega$, which modulates the size, $\delta$, of the diffusion-convection layer (Scheme 1):

$$\delta(\text{cm}) = 1.61 \times D(\text{cm}^2\text{s}^{-1})^{1/3} \times \nu(\text{cm}^2\text{s}^{-1})^{1/6}\omega(\text{rad s}^{-1})^{-1/2} \quad (1)$$

where $D$ is the diffusion coefficient, $\nu$ is the kinematic viscosity, and $\omega$ is the rotation rate.

The aim of the analysis is to predict the current/potential curves under the control of the various transport and reactivity factors sketched in Scheme 1. A popular way of representing these relationships is the so-called "Tafel plot" relating the log of the current, or current density, to the electrode potential or to the overpotential (difference between the electrode potential and the equilibrium potential of the reaction being catalyzed).[14] In the following report we will use current densities rather than currents. Historically, the Tafel equation is the irreversible version of the more general Butler–Volmer equation, which describes the relationship between the kinetics of an electrochemical charge-transfer reaction, represented by the log of the current or current density, and its thermodynamics, represented by the overpotential. The ensuing Tafel plots of such reactions are usually linear, in which case they are characterized by their slope and by the value of the exchange current density, i.e., the current density at overpotential zero. The Tafel slope is related to the electrochemical transfer coefficient, $\alpha$, in this case comprised between 0 and 1. This is often close to 0.5, which corresponds to a $F/2RT \ln 10$ Tafel slope. In fact the "Tafel" slope for electrocatalytic reactions in general, and in particular those depicted in Scheme 1, has no reason to systematically have such a value. The ensuing Tafel plots are not even necessarily linear. Strictly speaking, the current–potential relationships characterizing electrocatalytic systems, such as represented in Scheme 1, are not actual Tafel plots of electrochemical charge-transfer reactions. To conform to usage, we nevertheless retain the appellation Tafel plot in the very broad sense of a log current (or current density) vs overpotential relationship that would result from the interplay of the various rate-controlling factors of an electrocatalytic reaction. A methodology for describing the kinetics as a function of various controlling factors has been developed in the framework of RDEV for electrocatalytic electrode coatings in the 1980s.[7] It must, however, be extended in two directions to meet the requirements of the current study. The earlier approach was essentially focused on the catalytic plateau currents that are encountered with such systems at large overpotentials, whereas the study here is concerned with a description of the foot of the current–potential response, where


dx.doi.org/10.1021/ja403656w | J. Am. Chem. Soc. 2013, 135, 10492–10502

**Table 1. Characteristic Current Densities**[a]

| rate-controlling phenomenon | characteristic current density | parameters, remarks |
|---|---|---|
| catalytic reaction | $I_k = Fk_{cat}C_{cat}d_f$ | $k_{cat} = k_{2nd}C_{subtr}$: pseudo first-order rate constant of the catalytic reaction |
| proton−electron hopping | $I_{H,e} = \frac{FD_{H,e}C_{cat}}{d_f}$ | $D_{H,e}$: proton−electron hopping diffusion coefficient (see text) |
| proton diffusion in the film | $I_{H,in} = \frac{FD_{H,in}C^0_{H^+}}{d_f}$ | $D_{H,in}$: proton diffusion coefficient in the film |
| diffusion of the buffer components in the film | $I_{ZH,in} = \frac{FD_{ZH,in}C^0_{ZH}}{d_f}$ | $D_{Z,H,in}$, $D_{Z,in}$: diffusion coefficients of ZH and Z in the film |
| | $I_{Z,in} = \frac{FD_{Z,in}C^0_{Z}}{d_f}$ | |
| proton diffusion in the solution and fast equilibration at the film solution interface | $I_{H,out} = \frac{FD_{H,out}C^0_{H^+}}{\delta}$ | $D_{H,out}$: proton diffusion coefficient in the solution. |
| diffusion of the buffer components in the solution and fast equilibration at the film solution interface | $I_{ZH,out} = \frac{FD_{ZH,out}C^0_{ZH}}{\delta}$ | $D_{ZH,out}$, $D_{Z,out}$: diffusion coefficients of ZH and Z in the solution. |
| | $I_{Z,out} = \frac{FD_{Z,out}C^0_{Z}}{\delta}$ | |

[a] $d_f$: film thickness. $\delta$: diffusion layer thickness (eq 1). $C_{cat}$: total concentration of the catalyst in the film. $C_{subtr}$: concentration of substrate in the film. $C^0_H$,$C^0_{ZH}$,$C^0_Z$: concentrations of $H^+$, ZH, and Z in the solution, respectively.

the contribution of reactant transport in the solution is expected to be minimal, although not necessarily negligible. The other extension concerns the coupling between electron transfer and proton transfer in electrocatalytic films of the type shown in Scheme 1. PCET reactions have been the object of intense investigation during the past decade with particular emphasis on concerted proton−electron transfers (CPET) in which proton and electron are transferred during a single step.[6,15] In the electrocatalytic films under discussion, coupling between proton and electron transfers comes into play at two levels. One involves the proton−electron hopping through the film, which replaces the single electron hopping of previous studies. The other concerns the production of protons at the electrode from the oxidation of the reduced form of the catalyst (PH yielding Q + $H^+$) in the presence or absence of a buffer (ZH/Z).

Electrocatalytic films such as those that are object of the present analysis are porous structures where the solvent can penetrate and the substrate, products, solvated protons, and buffer components can diffuse freely in the pores. Proton−electron hopping conduction takes place in the solid sections of the structure where continuity is ensured even at the cost of dynamic percolation.[16] On the whole, the various elements of the structure can be averaged and considered as equivalent to a homogeneously distributed set of catalytic sites between which protons and electrons can hop in a coupled manner and through which substrate, products, solvated protons, and buffer components may diffuse freely through an equivalent isotropic film as sketched in Scheme 1 in a similar manner as already described for polymer electrode coatings.[17]

Additional assumptions, approximations, or restrictions are: (i) The analysis is restricted here to the case where catalysis and proton−electron hopping are performed by the same centers. If necessary, it could be extended to cases where the catalytic and the conduction centers are not the same as previously illustrated with electron-hopping examples. (ii) Proton−electron hopping through the film may follow a concerted pathway (CPET) that goes directly from PH to Q or two stepwise pathways, a PET pathway (proton transfer first, from PH to P, followed by electron transfer between P and Q) or a EPT pathway (electron transfer first, between PH and QH, followed by proton transfer, from QH to Q). We consider the case where the proton transfers involved in the stepwise pathways are fast and unconditionally at equilibrium. It is shown in the Supporting Information (SI) that all three pathways are equivalent. (iii) The electron-transfer reaction at the electrode regenerating Q from the oxidation of PH with production of a proton may likewise follow concerted or stepwise pathways. We consider the cases where the concerted reaction is fast and unconditionally at equilibrium and where the proton- and electron-transfer reactions are all fast and unconditionally at equilibrium in the stepwise pathways. (iv) As mentioned in the Introduction, the substrate, A, is assumed to be in large concentration in the solution and in the film, so large that it remains constant. (v) We further assume that the partition coefficients of $H^+$, ZH, and Z between the solution in the pores and the solution outside the film are approximately equal to unity.

In the following, each current density is defined as the current intensity divided by the projection of the real surface area on the geometrical electrode surface. It is convenient to represent each of the factors by a characteristic current density as summarized in Table 1. The expressions of these characteristic current densities result from the following analysis.

Proton−electron hopping through the film may be likened to a linear diffusional transport obeying the Fick's diffusional law as shown in the SI (1.1), assuming that there is no electric field effect within the film because the hopping process does not involve net charge transport. Association with the catalytic reaction (Scheme 1) leads to the following steady-state expressions of the Fick's law modified by a kinetic catalytic term.

$$D_{H,e}\frac{d^2C_{PH}}{dx^2} + k_{cat}C_Q = 0 \quad (2)$$

$$D_{H,e}\frac{d^2C_Q}{dx^2} - k_{cat}C_Q = 0 \quad (3)$$

where $x$ is the distance from the electrode and the $C$ is the concentration of the subscript species.

Insofar the proton-transfer steps are at equilibrium (condition ii above) eqs 2 and 3 apply irrespective of the mechanism of proton−electron hopping, albeit $D_{H,e}$ may have different expressions in each case (SI, 1.1).

Condition (iii) above implies that the following equivalent expressions of the Nernst law apply at the electrode surface ($x$ = 0):

$$\frac{(C_Q)_{x=0} \times (C_{H^+})_{x=0}}{(C_{PH})_{x=0} \times C^0} = \exp\left[\frac{F}{RT}(E - E^0_{Q+H^+/PH})\right]$$

$$\frac{(C_Q)_{x=0} \times (C_{ZH})_{x=0}}{(C_{PH})_{x=0} \times (C_Z)_{x=0}} = \exp\left[\frac{F}{RT}(E - E^0_{Q+ZH/PH+Z})\right]$$

where the two standard potentials characterizing the catalyst PH/Q couple are related by

$$E^0_{Q+ZH/PH+Z} = E^0_{Q+H^+/PH} + \frac{RT}{F}\ln\left(\frac{K_a}{C^0}\right) \quad (4)$$

($K_a$ is the acidity constant of ZH, $C^0$ is a normalizing concentration, conveniently taken as equal to 1 M.)

The above Nernst equations may also be expressed as a function of the overpotential $\eta = E - E^{eq}_A$, where $E^{eq}_A$ is the equilibrium potential of the reaction to be catalyzed. It is not necessarily a standard potential and may contain reactant concentration terms, as e.g., the pH, according to the reaction under consideration and to the most convenient definition the overpotential in each particular case.

Integration of eqs 2 and 3, taking into account the appropriate boundary conditions and noting that we are interested in what happens in the foot of the current responses, leads to (see SI 1.2, Table 1):

$$\frac{(C_Q)_{x=0}}{C_{cat}} = \frac{I}{\sqrt{I_k I_{H,e}}\tanh\left(\sqrt{\frac{I_k}{I_{H,e}}}\right)} \quad (5)$$

*1.1. High Buffer Concentrations (Insignificant Buffer Consumption Within the Catalyst Film).* Joint control by catalytic reaction and proton−electron hopping is observed when the concentration of buffer is so large that the concentrations of its two components are constant throughout the film. The buffer serves to neutralize the protons generated by the CPET electrode reaction and to convert, at least partially, their diffusion toward the solution into a ZH diffusion toward the solution and a diffusion of Z toward the electrode and, additionally, to participate as reactants to the CPET electrode reaction. Then the Tafel plots are predicted to obey the following equation (see SI 1.2):

$$\log I = \log I_0 + \frac{F}{RT\ln 10}\eta \quad (6)$$

where $I_0$, the current density at zero overpotential, can be considered as an exchange current density by analogy with electrochemical reaction Tafel plots. It can be expressed as:[18]

$$\log I_0 = \log\left[\frac{C^0}{C^0_{H^+}}\sqrt{I_k I_{H,e}}\tanh\left(\sqrt{\frac{I_k}{I_{H,e}}}\right)\right] + \frac{F(E^{eq}_A - E^0_{Q+H^+/PH})}{RT\ln 10}$$
$$= \log\left[F\frac{C^0}{C^0_{H^+}}C_{cat}k_{cat}d_f^{opt}\tanh\left(\frac{d_f}{d_f^{opt}}\right)\right] + \frac{F(E^{eq}_A - E^0_{Q+H^+/PH})}{RT\ln 10} \quad (7)$$

with

$$d_f^{opt} = \sqrt{\frac{D_{H,e}}{k_{cat}}} \quad (8)$$

The Tafel plots are thus predicted to have a $F/RT$ ln 10 slope and to depend on film thickness as pictured in Figure 1a. Below the optimal value, $d_f^{opt}$, the current density response increases in proportion to film thickness, whereas beyond $d_f^{opt}$, the response plateaus off. This is best represented as a variation of the exchange current density with the film thickness as shown in

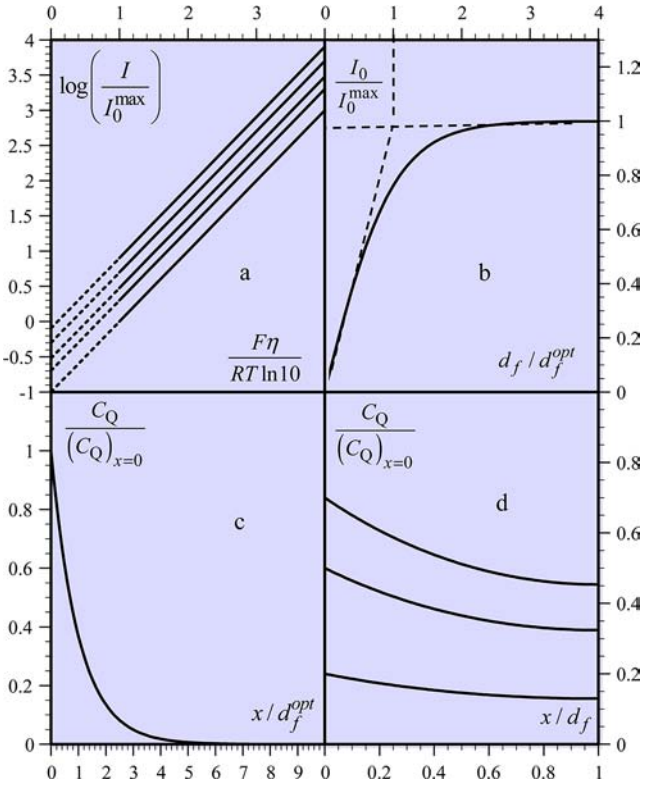


**Figure 1.** Large buffer concentrations. (a) Tafel plots predicted for a series of increasing thicknesses from bottom to top. (b) Variation of the current density with the film thickness (relative to the optimal film thickness, $d_f^{opt}$) at $\eta$ = 0. $I_0$ and $I_0^{max}$ are defined in eqs 7, 7′, 9 and 9′, respectively. For $d_f$ see eq 8. (c) Concentration profile of Q (relative to the concentration of Q at the electrode−film interface) for mixed control of the catalytic reaction and the diffusion-like proton−electron hopping under pure kinetic conditions for a film thickness $d_f = 10 \times d_f^{opt}$. (d) Concentration profile of Q (relative to catalyst concentration in the film) as a function of increasing electrode potential (from bottom to top) for a film of thickness equal to $d_f^{opt}$.


dx.doi.org/10.1021/ja403656w | J. Am. Chem. Soc. 2013, 135, 10492−10502

Figure 1b where the maximal value reached by $I_0$, noted $I_0^{max}$, may be expressed by[19]

$$I_0^{max} = F\frac{C^0}{C^0_{H^+}}C_{cat}\sqrt{k_{cat}D_{H,e}}\exp\left[\frac{F(E_A^{eq} - E^0_{Q+H^+/PH})}{RT}\right]$$
$$= F\frac{C^0}{C^0_{H^+}}C_{cat}k_{cat}d_f^{opt}\exp\left[\frac{F(E_A^{eq} - E^0_{Q+H^+/PH})}{RT}\right] \quad (9)$$

In other words, eq 7 may be recast as

$$I_0 = I_0^{max}\tanh\left(\frac{d_f}{d_f^{opt}}\right) \quad (10)$$

More rigorously, the variation of the exchange current density with the film thickness (Figure 1b) shows two limiting behaviors:

when $d_f/d_f^{opt} \to 0$: $I_0 \to I_0^{max}\frac{d_f}{d_f^{opt}}$

$$= F\frac{C^0}{C^0_{H^+}}C_{cat}k_{cat}\exp\left[\frac{F(E_A^{eq} - E^0_{Q+H^+/PH})}{RT}\right] \times d_f$$

The exchange current density is governed solely by the catalytic reaction, being consequently proportional to film thickness.

When $d_f/d_f^{opt} \to \infty$, then $I_0 \to I_0^{max}$

(as given by eq 10).

The exchange current density is then independent of film thickness, being under the mixed control of the catalytic reaction and the diffusion-like proton−electron hopping under "pure kinetic conditions".[20] Under these conditions, the concentration profile of Q (Figure 1c) is independent of the film thickness as a result of mutual compensation of catalytic reaction and diffusion-like proton−electron hopping. It is confined in a reaction-diffusion layer of $(D_{H,e}/k_{cat})^{1/2}$ thickness.

It follows that there is no advantage to continuing to increase the thickness much beyond $d_f^{opt}$. It suffices that $I_0$ reaches a value equal to $I_0^{max}$ within experimental uncertainty. As shown in Figure 1d, increasing the electrode potential shifts the position of the PH/Q+H$^+$ equilibrium at the electrode−film interface. This consequently leads to greater values of $C_Q$ throughout the film and a greater current density (Figure 1a).

We note that the current response is independent of the rotation rate. In other words the "Koutecky−Levich" (KL) plots are horizontal. KL plots in RDEV are plots of the inverse of current density against the inverse of the square root of the rotation rate.[21] In the present discussion they may be taken at any potential along the Tafel plot. When they are linear, the intercept is representative of phenomena occurring in the film, whereas the slope reflects reactant transport in the solution. This approach is actually not general because KL plots are not always linear. Examples of nonlinear KL plots have been given in the analysis of redox polymer film responses.[7] Observing a nonlinear KL plot does not mean that the events taking place in the film are not separable from transport in solution, but that it requires a somewhat less straightforward procedure. Examples will be given in the following analysis.

*1.2. Buffer-Free Conditions.* Nonlinear KL plots are observed when no buffer has been introduced in the solution, which represents the converse extreme of the case where the whole system was completely buffered as examined earlier. Then (see SI 1.2):

$$\frac{(C_{H^+})_{x=0}}{C^0_{H^+}} = I\left(\frac{1}{I_{H,in}} + \frac{1}{I_{H,out}}\right) + 1$$

(symbols are defined in Table 1). An extreme of a nonbuffered situation is when the production of protons at the electrode is much larger than the proton concentration in solution, i.e., $(C_{H^+})_{x=0} \gg C^0_{H^+}$, leading to

$$\frac{(C_{H^+})_{x=0}}{C^0_{H^+}} = I\left(\frac{1}{I_{H,in}} + \frac{1}{I_{H,out}}\right)$$

with

$$I_{H,in} = \frac{FD_{H,in}C^0_{H^+}}{d_f}, \quad I_{H,out} = \frac{FD_{H,out}C^0_{H^+}}{\delta}$$

In most cases the RDEV diffusion-convection layers, $\delta$, are larger than the catalyst film thickness, $d_f$ (of the order of $10^{-2}$−$10^{-3}$ cm against $10^{-4}$−$10^{-6}$ cm, respectively). Since the ratio of the diffusion coefficients is not very different from 1, $I_{H,in} \gg I_{H,out}$, and therefore:

$$\frac{(C_{H^+})_{x=0}}{C^0_{H^+}} = \frac{I}{I_{H,out}}$$

In this case, the diffusion of solvated protons out of the film controls the current density jointly with proton−electron hopping. The Tafel plots are then expected to obey eq 11 as represented in Figure 2a (see SI 1.2).

$$\log I = \frac{1}{2}\log(I_0 \times I_{H,out}) + \frac{F}{2RT\ln 10}\eta \quad (11)$$

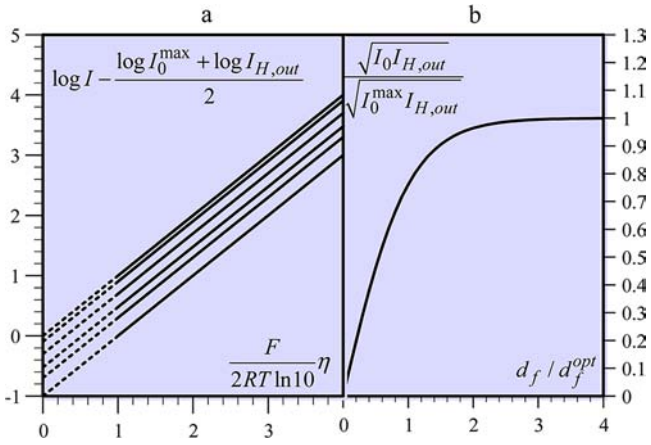


**Figure 2.** No buffer. (a) Tafel plots predicted for a series of increasing thicknesses from bottom to top. (b) Variation of the current density with the film thickness (relative to the optimal film thickness) at $\eta = 0$. $I_0$ and $I_0^{max}$ are defined in eqs 7, 7′, 9 and 9′, respectively. $I_{H,out}$ is defined in Table 1.

$I_0$ being given by eqs 7, 7′ or (9, 9′ and 10) and $I_{H,out}$, which characterizes the proton transport in solution, is defined in Table 1. In the first term of eq 11, $I_0$ is inversely proportional to $C^0_{H^+}$ (eq 7′), whereas $I_{H,out}$ is directly proportional to $C^0_{H^+}$ (Table 1) making the first term of eq 11 independent of pH. The Tafel plot predicted by eq 11 may, however, be pH dependent if $E_A^{eq}$, which


dx.doi.org/10.1021/ja403656w | J. Am. Chem. Soc. 2013, 135, 10492−10502

serves as reference in the definition of the overpotential, depends itself on pH.

The Tafel slope is $F/2RT$ ln 10. KL plots are not linear, even if they may look linear within the necessarily limited range of accessible rotation rates. Figure 3 illustrates this misleading state

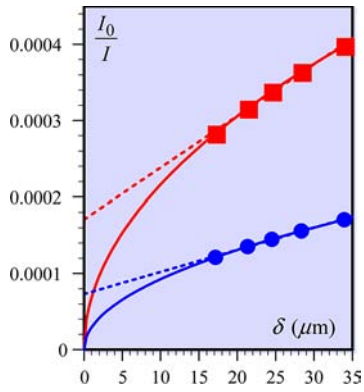


**Figure 3.** KL plots in absence of buffer: $I_0/I$ as function of diffusion layer thickness $\delta$, for two different values of the overpotential: $\eta$ = 0.4 (red squares) and 0.5 (blue dots) with $I_0 = 2 \times 10^{-10}$ A cm$^{-2}$, $D_{H,out} = 5 \times 10^{-5}$ cm$^2$ s$^{-1}$, $C^0_{H^+} = 10^{-6}$ M. Dots correspond to typical rotation rates: 2500, 1600, 1225, 900, and 625 rpm (using eq 1 with $\nu = 10^{-2}$ cm$^2$/s). Dotted lines correspond to purposely forced linear fitting of the data corresponding to rotation rates between 625 and 2500 rpm.

of affairs. It also shows that, in such a situation, the slope of the apparently linear KL relationship varies with the electrode potential unlike what is expected with truly linear KL relationships.

One could be tempted to define an exchange current density for this case as being the current density at overpotential zero. The "exchange current density" thus obtained, $(I_0 \times I_{H,out})^{1/2}$ is, however, somewhat unusual as compared to conventional electrochemical reactions in the sense that it incorporates the rate of proton transport in the solution and therefore depends on the RDEV rotation rate (through $I_{H,out}$ and eq 1).

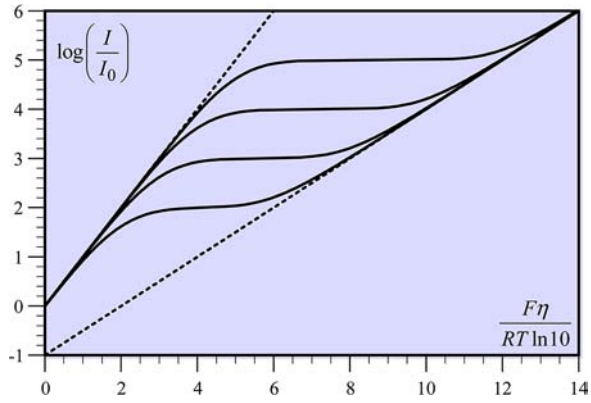


**Figure 4.** Tafel plots (full lines) predicted for intermediate buffer concentrations, showing the passage from joint control by catalytic reaction and proton–electron hopping (upper dotted line) to joint control by catalytic reaction, proton–electron hopping, and proton diffusion (lower dotted line) for a series of $I_{Z,out}/I_0$ values (10, 100, 1000, 10 000, 100 000 from bottom to top) corresponding to increasing value of buffer concentration ($I_{Z,out} = FD_{Z,out}C^0_Z/\delta$). Figure has been plotted for the following values of the other parameters: $C^0_{ZH}/C^0_Z = 1$ (the pH is equal to the ZH p$K_a$) and $I_0/I_{H,out} = 100$.

This exchange current density varies with the film thickness as shown in Figure 2b, first proportionally for $d_f \ll d_f^{opt}$ then reaching saturation with a value $(I_0^{max} \times I_{H,out})^{1/2}$ in which the expression of $I_0^{max}$ is the same as in eqs 9 and 9′ introduced previously in the case of perfect buffering.

*1.3. Intermediate Buffer Concentrations.* For intermediate buffer concentrations, the same assumptions concerning proton transfer and transport lead to a general implicit expression of the Tafel plots given by eq 12 (see SI 1.2):

$$\frac{F}{RT\ln 10}\eta = \log\left(\frac{I}{I_0}\right) + \log\left[\frac{I_{Z,out}}{I_0}\frac{I_0}{I_{H,out}}\frac{\left(\frac{I}{I_0}\frac{I_0}{I_{Z,out}} - 1\right) + \sqrt{\left(\frac{I}{I_0}\frac{I_0}{I_{Z,out}} - 1\right)^2 + 4\left(\frac{I}{I_0}\frac{I_0}{I_{Z,out}} + \frac{C^0_{ZH}}{C^0_Z}\right)\frac{C^0_Z}{C^0_{ZH}}\frac{I_{Z,out}}{I_0}\frac{I_0}{I_{H,out}}}}{2}\right] \quad (12)$$

The exchange current density, $I_0$, is defined by eqs 7, 7′ or 9, 9′ and 10. The buffer base and proton solution transport characteristic currents, $I_{Z,out}$ and $I_{H,out}$ respectively, are defined in Table 1.

Equation 12 allows the construction of a typical series of such Tafel plots as shown in Figure 4. It is seen that, at a given value of the buffer concentration, the high-buffer behavior tends to be reached at low overpotentials, whereas the no-buffer behavior tends to be reached oppositely at high overpotentials. In between these two limits the Tafel plots plateaus off. The current density is then $I = I_{Z,out}$, obtained when the concentration of the buffer base at the electrode surface comes close to zero as a result of the reaction with the catalytically generated protons. The current response is then solely controlled by the transport of the buffer base from the solution toward the film.

One conclusion of this section is that the combination of the various controlling factors, catalytic reaction, and proton–electron hopping conduction through the film as well as proton transfer and transport may result in quite different Tafel slopes, $F/RT$ ln 10, $F/2RT$ ln 10 or 0. Tafel plots such as those represented in Figure 4 are quite unusual if one refers to conventional electrochemical reactions. Illustrating experimental examples of such behaviors are given in the next section, which is devoted to application of the above analyses and equations to an illustrative experimental example.

**2. Application to a Cobalt-Based $O_2$-Evolution Catalyst.** The cobalt-based $O_2$-evolution catalyst may be analyzed according to Scheme 1 and the ensuing methodology simply considering that $k_{cat} = 4 \times k_C$ in eqs 2 and 3. In this analysis, the overpotential is defined as

$$\eta = E - E^{eq}_{O_2/H_2O} \text{ with}$$

$$E^{eq}_{O_2/H_2O} = E^0_{O_2/H_2O} - \frac{RT\ln 10}{F}\left(pH - \frac{1}{4}\log\left(\frac{P_{O_2}}{P^0}\right)\right) \quad (13)$$


dx.doi.org/10.1021/ja403656w | J. Am. Chem. Soc. 2013, 135, 10492–10502

and $E^0_{O_2/H_2O}$ = 1.23 V vs NHE.[22] A series of RDEV experiments was carried as a function of two main parameters, the concentration of the buffer (including the absence of buffer) and the film thickness. The stationary current density was measured point by point at a series of decreasing electrode potential values and at different rotation rates.

*2.1. High Buffer Concentrations (≥100 mM $P_i$).* In presence of a large amount of buffer (0.1 M $NaP_i$ at pH 7), Tafel plots with a $F/RT$ ln 10 (1/59 mV at 297 K) slope are obtained for a series of film thicknesses (Figure 5a). They were observed to be

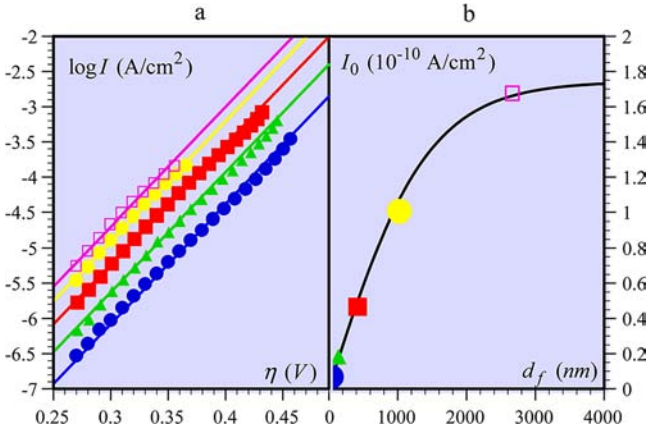


**Figure 5.** (a) Tafel plots of Co–OEC films operated in 0.1 M $KP_i$ pH 7 electrolyte with increasing film thicknesses: 40 nm (blue dots), 120 nm (green triangles), 400 nm (red squares), 1024 nm (yellow diamonds), 2665 nm (magenta open squares) (for the estimation of the film thickness, see Experimental Section). Rotation rate: 1000 rpm. The slope of the solid lines is $F/RT$ ln 10. (b) Variation of the exchange current density with the film thickness. Solid line: fitting according to $I_0 = I_0^{max}\tanh(d_f/d_f^{opt})$ (eq 10).

independent of rotation rates (from 625 to 2500 rpm). The current density increases with film thickness before reaching saturation (Figure 5a). These observations are what is anticipated for joint control by the catalytic reaction and by proton–electron hopping as discussed in the preceding section.

The variation of the Tafel intercept at $\eta = 0$ (exchange current density) is thus expected to follow the variation shown in Figure 1b and to obey eqs 7, 7′, 8, 9, and 9′. This is what is indeed seen in Figure 5b, while application of these eqs 7–9 leads to

$$d_f^{opt} = \sqrt{\frac{D_{H,e}}{k_{cat}}} = 1440 \text{ nm} \quad (14)$$

and

$$I^{max}_{0,pH=7} = 1.75 \times 10^{-10} \text{A/cm}^2 \quad (15)$$

on the understanding that $E^{eq}_{A,pH=7}$ is then given by eq 13 with $P_{O_2}/P^0$ = 0.2 and pH = 7, i.e., $E^{eq}_{A,pH=7}$ = 0.807 V vs NHE.

*2.2. Buffer-Free Conditions.* Tafel plots acquired at pH 6 in absence of buffer display a $F/2RT$ ln 10 slope at various rotation rates for various film thicknesses (Figure 6). In this case the overpotential is defined using a value of $E^{eq}_{O_2/H_2O}$ corresponding to pH 6 by application of eq 13 ($E^{eq}_{A,pH=6}$ = 0.866 V vs NHE). These data are distinct from the background currents associated with the RDE surface alone and are unaltered with changing the ionic strength, supporting electrolyte, or the elimination of $CO_2$, and therefore carbonate, from the electrolyte. It clearly appears that

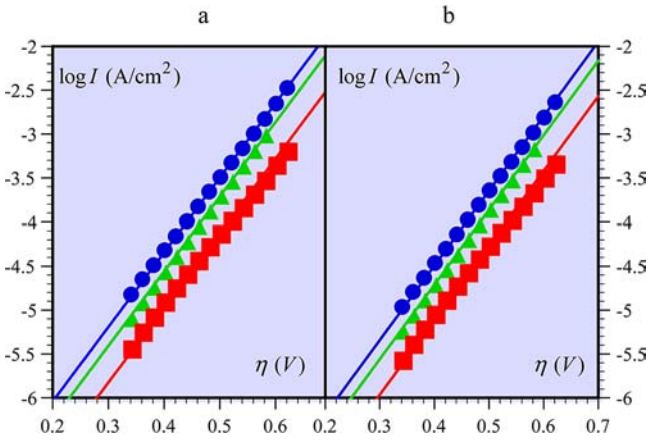


**Figure 6.** Tafel plots of Co–OEC films operated in 0.1 M $NaClO_4$ pH 6 electrolyte with no buffer present as a function of film thickness (in nm) 48 (red squares), 200 (green triangles), 575 (blue dots) at two rotation rates. (a) 2500 and (b) 625 rpm (data at other rotation rates are given in the SI). The slope of the solid lines is $F/2RT$ ln 10.

the response is dependent on film thickness thus ruling out a limitation by the PCET kinetics at the electrode surface. As detailed in the preceding section, the $F/2RT$ ln 10 slopes are coherent with a catalytic PCET process with water as proton acceptor associated with proton–electron hopping and jointly controlled by proton diffusion toward the solution in the absence of buffer. The intercept, logarithm of the current density at zero overpotential, is then $\log((I_{H,out} \times I_0)^{1/2})$. It allows access to the same intrinsic information on the system as in the high buffer concentration situation, yet taking into account the diffusion properties of the proton as required for the estimation of $I_{H,out}$. Because it is partially controlled by proton diffusion toward the solution, the current response is sensitive to the rotation rate of the electrode. This dependence is reported quantitatively in Figure 7a where the variation of $I_{H,out} \times I_0$ with $1/\delta$ is displayed

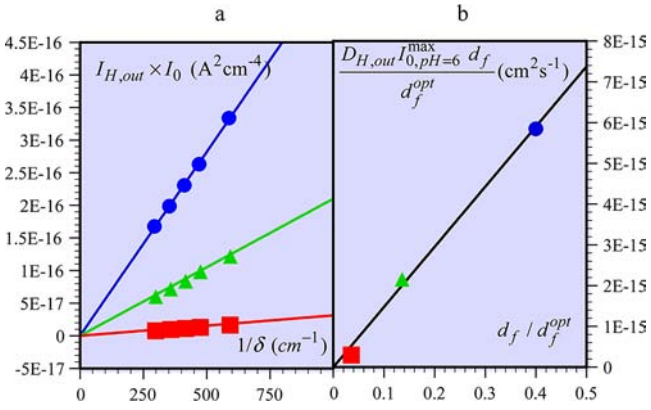


**Figure 7.** (a) $I_{H,out} \times I_0$ as function of $1/\delta$ (using eq 1 with $D = 5 \times 10^{-5}$ cm²/s and $\nu = 10^{-2}$ cm²/s)[21] for films of various thicknesses (in nm) 48 (red square), 200 (green triangles), 575 (blue dots). (b) Slopes of the straight lines in (a).

and indeed obeys the simple proportionality predicted from the application of eq 10 and the definition of $I_{H,out}$ in Table 1:

$$I_{H,out} \times I_0 = FD_{H,out}C^0_{H^+}I^{max}_{0,pH=6}\tanh\left(\frac{d_f}{d_f^{opt}}\right) \times \frac{1}{\delta}$$

Since the three films examined in Figure 7 are much thinner than $d_f^{opt}$ (1440 nm), the above equation becomes

$$I_{H,out} \times I_0 = FD_{H,out}C_{H^+}^0 I_{0,pH=6}^{max} \frac{d_f}{d_f^{opt}} \times \frac{1}{\delta}$$

A simple proportionality to film thickness is indeed observed as reported in Figure 7b, which plots the slopes of the straight lines in Figure 7a against the film thickness under the form of a $D_{H,out}I_{0,pH=6}^{max}/d_f^{opt}$ vs $d_f/d_f^{opt}$ diagram, the slope of which, $D_{H,out}I_{0,pH=6}^{max}/d_f^{opt}$, may be used to estimate $D_{H,out}$, after $I_{0,pH=6}^{max}$ = $1.75 \times 10^{-10}$ A/cm$^2$, equal to $I_{0,pH=7}^{max}$ (eq 15) by application of eq 9′. The value thus obtained for $D_{H,out}$, $8.5 \times 10^{-5}$ cm$^2$/s, is in excellent agreement with literature values ($9.3 \times 10^{-5}$ cm$^2$/s),[23] showing the excellent consistency of the data obtained with high buffer concentrations on the one hand and those obtained with no buffer at all on the other.

The effect of varying the pH is displayed in Figure 8.[24] As shown in the first section (eq 11), the variation of the Tafel plots

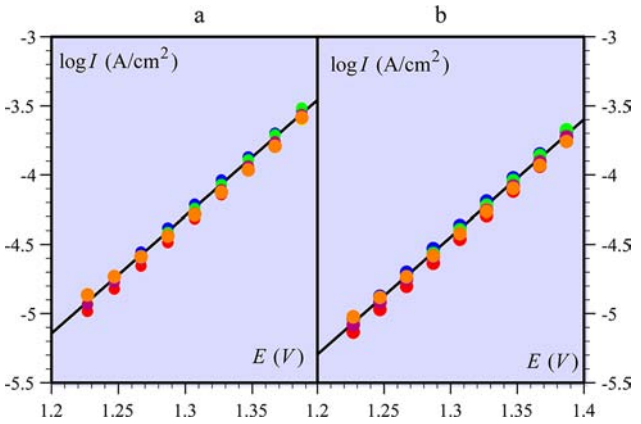


**Figure 8.** Tafel plots of a 200 nm Co−OEC films operated in operated in 0.1 M $NaClO_4$ with no buffer present, pH: 6.0 (blue), 6.2 (green), 6.4 (red), 6.6 (yellow), 6.8 (magenta), 7.2 (orange), at two rotation rates. (a) 2500 and (b) 625 rpm (data at other rotation rates are given in the SI). The slopes of the straight lines are $F/2RT$ ln 10.

with pH are predicted to follow the variation of $E_A^{eq} = E_{O_2/H_2O}^{eq}$ (eq 13), which served as reference for the definition of the overpotential. The results are therefore best represented by plotting log $I$ vs the electrode potential, $E$, rather than vs $\eta$, leading as expected to a pH-independent plot as indeed seen in Figure 8.

*2.3. Weakly Buffered Electrolytes (0.3−10 mM $P_i$).* The mechanism thus established is further confirmed by the results obtained in weakly buffered solutions, which are displayed in Figure 9. The Tafel plots there are strikingly similar to the predictions displayed in Figure 4. Whereas a $F/RT$ ln 10 slope is observed at low overpotential, a $F/2RT$ ln 10 slope is observed at high overpotential with a transition that depends both on buffer concentration and rotation rate. From the intercepts of the $F/RT$ ln 10 slope straight lines we obtain $I_0 = 2.7 \times 10^{-11}$ A/cm$^2$ in agreement with the data shown in Figure 5b, and from the intercepts of the $F/2RT$ ln 10 slope straight lines we obtain $I_{H,out} \times I_0$ as a function of $1/\delta$, thus leading to $D_{H,out} = 8 \times 10^{-5}$ cm$^2$/s in full agreement with the previous buffer-free experiments.

The knowing $I_0$ as well as $I_{H,out}$ at each rotation rate, the whole set of data can be fit at any buffer concentration with a single parameter, $D_{Z,out}$, through $I_{Z,out} = FD_{Z,out}C_Z^0/\delta$ according to eq 12. This is in line with the fact that the transition between both

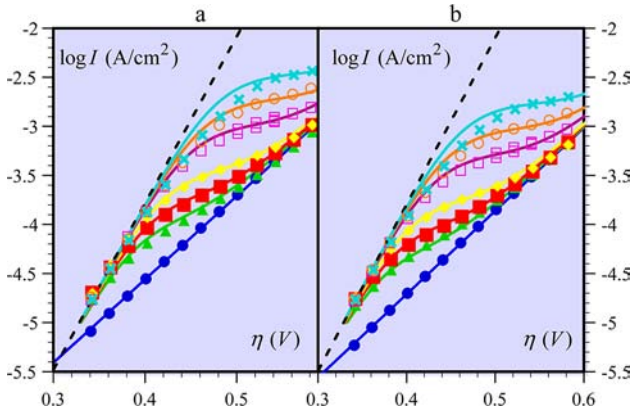


**Figure 9.** Tafel plots of a 200 nm Co−OEC films operated in 0 (blue dots), 0.3 (green solid triangles), 0.55 (red solid squares), 1 (yellow solid diamonds), 3 (magenta open squares), 5.5 (orange open diamonds), 10 (cyan cross) mM $NaP_i$ pH 6 electrolyte with 0.1 M $NaClO_4$ as supporting electrolyte at various rotation rate. (a) 2500 and (b) 625 rpm data at other rotation rates are given in the SI). The slopes of the straight lines are $F/RT$ ln 10 (dashed black) and $F/2RT$ ln 10 and (solid blue).

limiting behaviors is controlled by buffer diffusion in solution.[25] Fitting, as shown in Figure 9 leads to $D_{Z,out} = 6 \times 10^{-6}$ cm$^2$/s in agreement with literature values of the diffusion coefficient of $PO_4H^{2-}$ ($7.6 \times 10^{-6}$ cm$^2$/s).[26]

The effect of film thickness was systematically investigated at a low $P_i$ concentration (3 mM) at pH 6 at various rotation rates (Figure 10). The data are satisfactorily fitted with eq 12 using the

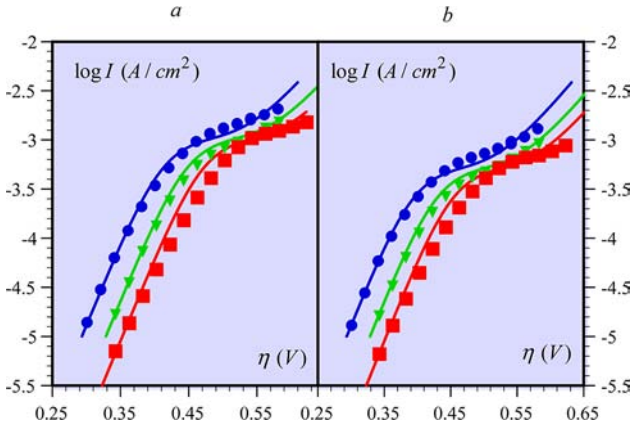


**Figure 10.** Tafel plots of Co−OEC films operated in 3 mM $NaP_i$ pH 6 electrolyte with 0.1 M $NaClO_4$ as supporting electrolyte with increasing film thicknesses (red squares) 48 (green triangles) 200 (blue dots) 575 nm at various rotation rate. (a) 2500 and (b) 625 rpm (data at other rotation rates are given in the SI). The solid colored lines correspond to fitting of data.

same diffusion parameters as above, i.e. $D_{H,out} = 8 \times 10^{-5}$ cm$^2$/s and $D_{Z,out} = 6 \times 10^{-6}$ cm$^2$/s as well as the same intrinsic parameter $I_{0,pH=6}^{max} = 1.75 \times 10^{-10}$ A/cm$^2$. This confirms the full consistency of our proposed mechanism.

*2.4. Kinetic and Thermodynamic Parameters of Co−OEC.* One remarkable aspect of our mechanistic analysis is that the data obtained at high buffer concentrations, with no buffer at all and in weakly buffered solutions, are perfectly consistent being in agreement with the same set of kinetic and thermodynamic characteristics. It is worth having a closer look at what can be


dx.doi.org/10.1021/ja403656w | J. Am. Chem. Soc. 2013, 135, 10492−10502

precisely derived from the experimental data in terms of kinetic and thermodynamic characteristics. The rate constant of the catalytic reaction, $k_{cat}$, the equivalent diffusion coefficient of proton−electron hopping, $D_{H,e}$ and the standard potential of the catalyst, $E^0_{Q+ZH/PH+Z}$ (or $E^0_{Q+H^+/PH}$) are three unknowns related by two equations deriving from the experimental determination of $D_{H,e}/k_{cat}$ from $d_f^{opt}$ (eq 8) and $k_{cat}C_{cat}\exp[-(F/RT)(E^0_{Q+ZH/PH+Z}$ or $E^0_{Q+H^+/PH})]$ from $I_0^{max}$ (eq 9). At the present stage, we do not know these three parameters independently from one another. Progress in this direction will most probably require resorting to faster electrochemical techniques in order to sense the proton−electron hopping rate in conditions where catalysis is made negligible. For the time being, knowing the combined parameter $k_{cat}C_{cat}\exp[-(F/RT)(E^0_{Q+ZH/PH+Z}$ or $E^0_{Q+H^+/PH})]$ will nevertheless allow the benchmarking of catalysts for a given reaction similar to the recently advocated comparison between turnover frequencies at zero overpotential.[27] In the present case of a catalytic film whose thickness may be varied, the proton−electron conduction is an additional benchmarking factor: the larger $D_{H,e}/k_{cat}$, the more globally efficient the catalysis. The optimal thickness, $d_f^{opt} = (D_{H,e}/k_{cat})^{1/2}$ being determined experimentally and the actual film thickness being adjusted to this value, the global benchmarking factor may then be derived from $I_0^{max}$ as

$$F\sqrt{D_{H,e}k_{cat}}\,C_{cat}\,\exp[-(F/RT)(E^0_{Q+ZH/PH+Z}\text{ or }E^0_{Q+H^+/PH})]$$

## EXPERIMENTAL SECTION

**Materials.** $Co(NO_3)_2{\cdot}6H_2O$ 99.999% (Strem) and $NaClO_4$ 99.99% metals basis (Aldrich) were used as received. $NaH_2PO_4$ 99%, $KH_2PO_4$ 99%, NaOH 99%, KOH 88%, and $KNO_3$ 99.0−100.5% were reagent grade and used as received from Macron. All $H_2O$ electrolyte solutions were prepared with type I water (EMD Millipore, 18.2 MΩ cm resistivity).

*Electrochemical Methods.* All electrochemical experiments were conducted using a CH Instruments 760C or 760D bipotentiostat, a BASi Ag/AgCl reference electrode (soaked in saturated NaCl), and a Pt-mesh counter electrode. Measurements were conducted using a Pine Instruments MSR rotator and a 5 mm diameter Pt-disk rotating electrode (RDE). Electrochemical experiments were performed using a three-electrode electrochemical cell with a porous glass frit separating the working and auxiliary compartments. Experiments were performed at room temperature (24 ± 1 °C) and electrode potentials were converted to the NHE scale using $E(NHE) = E(Ag/AgCl) + 0.197$ V.

**Film Preparation.** Catalyst films were prepared via controlled-potential electrolysis of 0.1 M potassium phosphate ($KP_i$), pH 7.0 electrolyte solutions containing 0.5 mM $Co^{2+}$. To minimize precipitation of cobalt(II) phosphate, 25 mL of 0.2 M $KP_i$ was added to 25 mL of 1.0 mM $Co^{2+}$ solution. The solutions thus prepared remained clear over the course of all depositions. Depositions were carried out using a 5 mm diameter Pt disk as the working electrode. Deposition by controlled potential electrolysis was carried out on quiescent solutions at 1.047 V without *i*R compensation. A typical deposition lasted 40 min for a 24 mC/cm$^2$ film (~200 nm thick). Following deposition, films were rinsed thoroughly in type I water to remove any adventitious $Co^{2+}$ and $P_i$. Thinner films were deposited under identical conditions but with passage of the desired amount of charge. Evaluation of film thickness was performed from an estimation of the volume occupied by each Co atom as previously described.[12] The amount of mol Co/cm$^2$ was determined from ICP analysis of films digested in 2% nitric acid (Fluka TraceSelect). Film thicknesses of 40, 120, 390, 1025, and 2665 nm (as shown in Figure 5) correspond respectively to 5, 15, 30, 150, and 400 mC/cm$^2$ deposition.

*Potentiostatic Tafel Data Collection in Well-Buffered $P_i$ Electrolyte.* Current−potential data were obtained by controlled potential electrolysis of 0.1 M $KP_i$ electrolyte pH 7.0 at a variety of applied potentials. Prior to film deposition, the solution resistance of the electrolyte to be used for Tafel data collection was measured using the *i*R test function. The electrolysis solution was exchanged for $Co^{2+}$-containing $KP_i$ electrolyte, without modifying the relative positions of the working and reference electrodes. The film was prepared by controlled potential electrolysis as described above. Following film preparation, the working electrode was rinsed in water and transferred, without drying, to the same electrolysis bath in which the solution resistance was measured. The electrode was allowed to equilibrate with the electrolysis solution for 5 min while being held at the open circuit potential. The rotation rate was set to 1000 rpm, and steady-state currents were then measured at applied potentials that descended from 1.267 to 1.097 V in 10 mV steps. For current densities greater than 10 μA cm$^{-2}$, a steady state was reached at a particular potential in <400 s. For current densities lower than 10 μA cm$^{-2}$, longer electrolysis times (15−20 min) were utilized to ensure that a steady state had been achieved. The solution resistance measured prior to the data collection was used to correct the Tafel plot for ohmic potential losses.

*Tafel Data in Low [$P_i$] Electrolyte, pH 6.* A 24 mC/cm$^2$ catalyst film was prepared onto a Pt RDE as described above. Following Tafel data acquisition in 0.1 M $KP_i$ electrolyte (Section 1.4), the electrode was rinsed thoroughly with type I water, and steady state current densities were acquired in weakly buffered electrolytes (1.0 M $NaClO_4$, pH 6 electrolyte containing [$NaP_i$] between 30 mM and 0.1 μM) with *i*R compensation (measured prior to film deposition) at rotation rates of 2500, 1600, 1225, 900, and 625 rpm at 20 mV intervals over the desired potential range. When necessary 0.5−5 μL aliquots of 1 M aqueous NaOH were added periodically to ensure minimal drift in bulk pH (±0.01) over the course of the experiment. The experiment was repeated twice more using the same catalyst film. Consecutive runs displayed excellent reproducibility. Following operation in $P_i$-free electrolyte the electrode was rinsed, and data acquisition was repeated in 0.1 M $KP_i$ electrolyte, as described above.

*Background Pt RDE Tafel Data.* Tafel data were acquired using a Pt RDE in the absence of a catalyst film. The electrode surface was polished to a mirror finish with 0.05 μm alumina, sonicated for 2 min, rinsed in 1 M $H_2SO_4$, and rinsed thoroughly in type I water. Those data were compared to data acquired with a 24 mC/cm$^2$ catalyst film deposited onto a Pt RDE and operated in 1 M $NaClO_4$ pH 7.0 electrolyte. Between 1.39 and 1.2 V the current measured with the catalyst film is 1 order of magnitude higher than the current measured on Pt in the absence of a catalyst film.

*Tafel Data in $P_i$-Free Electrolyte, pH 6.* A 24 mC/cm$^2$ catalyst film was prepared onto a Pt RDE as described above. Following Tafel data acquisition in 0.1 M $KP_i$ electrolyte, the electrode was rinsed thoroughly with type I water, and steady-state current densities were acquired in $P_i$-free 1 M $NaClO_4$ pH 6.0 electrolyte in a manner identical to that described above. Experiments were repeated for films operated in 0.5 M $NaClO_4$ and 1.0 M $KNO_3$. Within experimental uncertainty (less than the size of data points), data acquired are identical irrespective of electrolyte concentration or composition. To compare data in an electrolyte, completely lacking dissolved $CO_2$ and carbonate, $O_2$ was bubbled through a 1.0 M $NaClO_4$ solution overnight (>12 h), and data were acquired as described previously. Data arising from this measurement were identical to that acquired in 1 M $NaClO_4$ without bubbling $O_2$, indicating that dissolved carbonate species do not play a role in proton transfers during $O_2$ evolution in $P_i$-free media.

## CONCLUSION

A methodology has been established to predict the current responses expected in RDEV for the semi-general catalytic reaction scheme depicted in Scheme 1. The predictions concern the Tafel plots and their dependency on buffer concentration (including absence of buffer), film thickness and rotation rate, which are the main operational parameters that can be experimentally varied to uncover the reaction mechanism and determine its kinetic characteristics. To avoid unmanageable complexity, the scheme investigated is not general, but it can be

easily implemented for other reactions and controlling factors along the same principles, thanks particularly to the use of characteristic current densities that stand for each particular rate-governing factor involved. One important outcome of the theoretical analysis, whose pertinence is confirmed experimentally, is that the Tafel plots may have a variety of slopes, $F/RT$ ln 10, $F/2RT$ln10, 0, that not only may be observed along the whole plot but may also coexist within the overpotential range of a single plot. It is also remarkable that KL plots, relating the inverse of the current density to the inverse of the square root of the rotation rate, are not always linear, making somewhat more cumbersome, albeit still reachable, the separation of the events inside the film from reactant transport in the solution.

Application to water oxidation by films of a cobalt-based oxidic catalyst had a double purpose. One was to provide an experimental example of the viability of the proposed methodology and of its ability to uncover the reaction mechanism and determine its kinetic characteristics. The second was to actually establish kinetic characteristics of this particular catalyst in action, with a new focus on elucidating the reasons for the previously observed behavior in buffer-free electrolytes and the effect of film thickness on OER activity. Moreover, this catalyst seems to be a premiere in the field of catalytic electrode coatings designed for the activation of small molecules required for the resolution of modern energy challenges and this work may therefore serve as a methodological model for future studies.

Some of the features of the cobalt-based oxidic catalyst are remarkable and are worth emphasizing as they could be found with other catalysts of the same reaction or with other OECs or in other catalytic reactions. One of these is that the current response is controlled jointly by the catalytic reaction and proton−electron hopping. This mixed control results in an optimal thickness beyond which any increase is at best useless or may even afford rapidly diminishing returns in net catalytic activity.

Empirically one feels that the best catalysts correspond to a high catalytic rate constant, a high catalyst concentration in the film, a low catalyst standard potential, and also a fast proton−electron hopping conduction in the film. However what counts eventually is the value of the above combination of all these parameters into a global benchmarking index. The exact expression of the benchmarking index depends on the catalytic electron and proton stoichiometries, which are reflected in the Tafel slopes and $H^+$ reaction order, respectively.[25b] When the stoichiometries are the same a single index can be used. In the other case, the comparison should involve entire Tafel plots with the possibility that the first catalyst is better than the second in a certain range of overpotentials or pH and vice versa. Furthermore, if the catalyst is to be employed in a photoelectrochemical cell, the matching requirements of the targeted semiconductor substrates/assemblies will define the appropriate catalyst to be used.[28]

Deconvolution of the kinetics of the catalytic reaction and of proton−electron hopping conduction is a necessary requirement for a future assessment of the catalytic and conduction mechanisms that may a priori involve stepwise or concerted pathways. Examination of kinetic H/D isotope effects should also be useful in this endeavor.

## ■ ASSOCIATED CONTENT

### Supporting Information

Analysis of the kinetic responses and additional data. This material is available free of charge via the Internet at http://pubs.acs.org.

## ■ AUTHOR INFORMATION


### Corresponding Author

cyrille.costentin@univ-paris-diderot.fr; dnocera@fas.harvard.edu; saveant@univ-paris-diderot.fr


### Notes

The authors declare no competing financial interest.

## ■ ACKNOWLEDGMENTS

Part of this work was supported by a grant from the D.O.E., U.S. D.O.E. Grant DE-SC0009565

## ■ REFERENCES


(1) (a) Hoffert, M. I.; Caldeira, K.; Jain, A. K.; Haites, E. F.; Harvey, L. D. D.; Potter, S. D.; Schlesinger, M. E.; Schneider, S. H.; Watts, R. G.; Wigley, T. M. L.; Wuebbles, D. J. *Nature* **1998**, *395*, 881. (b) Nocera, D. G. *Inorg. Chem.* **2009**, *48*, 10001. (c) Abbott, D. *Proc. IEEE* **2010**, *98*, 42. (d) Chu, S.; Majumdar, A. *Nature* **2012**, *488*, 294.

(2) (a) Bard, A. J.; Fox, M. A. *Acc. Chem. Res.* **1995**, *28*, 141. (b) Lewis, N. S.; Nocera, D. G. *Proc. Natl. Acad. Sci. U.S.A.* **2006**, *103*, 1529. (c) Liu, F.; Concepcion, J. J.; Jurss, J. W.; Cardolaccia, T.; Templeton, J. L.; Meyer, T. J. *Inorg. Chem.* **2008**, *47*, 1727. (d) Barber, J. *Chem. Soc. Rev.* **2009**, *38*, 185. (e) Cook, T. R.; Dogutan, D. K.; Reece, S. Y.; Surendranath, Y.; Teets, T. S.; Nocera, D. G. *Chem. Rev.* **2010**, *110*, 6474.

(3) (a) Schneider, J.; Jia, H.; Muckerman, J. T.; Fujita, E. *Chem. Soc. Rev.* **2012**, *41*, 2036. (b) Costentin, C.; Robert, M.; Savéant, J.-M. *Chem. Soc. Rev.* **2013**, *42*, 2423. (c) Smieja, J. M.; Sampson, M. D.; Grice, K. A.; Benson, E. E.; Froehlich, J. D.; Kubiak, C. P. *Inorg. Chem.* **2013**, *52*, 2484.

(4) (a) Savéant, J.-M. *Chem. Rev.* **2008**, *108*, 2348. (b) Suntivich, J.; May, K. J.; Gasteiger, H. A.; Goodenough, J. B.; Shao-Horn, Y. *Science* **2011**, *334*, 1383.

(5) Gasteiger, H. A.; Marković, N. M. *Science* **2009**, *324*, 48.

(6) (a) Proton-Coupled Electron Transfer. Thematic Issue. *Chem. Rev.* **2010**, *110*, 6937. (b) Savéant, J.-M. *Energy Environ. Sci.* **2012**, *5*, 7718.

(7) (a) Andrieux, C. P.; Dumas-Bouchiat, J.-M.; Savéant, J.-M. *J. Electroanal. Chem.* **1982**, *131*, 1. (b) Andrieux, C. P.; Savéant, J.-M. *J. Electroanal. Chem.* **1982**, *134*, 163. (c) Andrieux, C. P.; Dumas-Bouchiat, J.-M.; Savéant, J.-M. *J. Electroanal. Chem.* **1984**, *169*, 9. (d) Andrieux, C. P.; Savéant, J.-M. In *Molecular Design of Electrode Surfaces*; Murray, R. W., Ed.; John Wiley and Sons: New York, NY, 1992; Vol. 22, p 207−270. (e) Savéant, J.-M. *Elements of molecular and biomolecular electrochemistry: an electrochemical approach to electron transfer chemistry*; John Wiley & Sons: Hoboken, NJ, 2006.

(8) (a) Kanan, M. W.; Nocera, D. G. *Science* **2008**, *321*, 1072−1075. (b) Kanan, M. W.; Surendranath, Y.; Nocera, D. G. *Chem. Soc. Rev.* **2009**, *38*, 109. (c) Dincă, M.; Surendranath, Y.; Nocera, D. G. *Proc. Natl. Acad. Sci. U.S.A.* **2010**, *107*, 10337. (d) Bediako, D. K.; Lassalle-Kaiser, B.; Surendranath, Y.; Yano, J.; Yachandra, V. K.; Nocera, D. G. *J. Am. Chem. Soc.* **2012**, *134*, 6801.

(9) (a) Steinmiller, E. M. P.; Choi, K.−S. *Proc. Natl. Acad. Sci. U.S.A.* **2009**, *106*, 20633. (b) Zhong, D. K.; Gamelin, D. R. *J. Am. Chem. Soc.* **2010**, *132*, 4202. (c) Pijpers, J. J. H.; Winkler, M. T.; Surendranath, Y.; Buonassisi, T.; Nocera, D. G. *Proc. Natl. Acad. Sci. U.S.A.* **2011**, *108*, 10056−10061. (d) Reece, S. Y.; Hamel, J. A.; Sung, K.; Jarvi, T. D.; Esswein, A. J.; Pijpers, J. J. H.; Nocera, D. G. *Science* **2011**, *334*, 645.

(10) (a) Lutterman, D. A.; Surendranath, Y.; Nocera, D. G. *J. Am. Chem. Soc.* **2009**, *131*, 3838. (b) Surendranath, Y.; Lutterman, D. A.; Liu, Y.; Nocera, D. G. *J. Am. Chem. Soc.* **2012**, *134*, 6326.

(11) (a) McAlpin, J. G.; Surendranath, Y.; Dincă, M.; Stich, T. A.; Stoian, S. A.; Casey, W. H.; Nocera, D. G.; Britt, R. D. *J. Am. Chem. Soc.* **2010**, *132*, 6882. (b) Kanan, M. W.; Yano, J.; Surendranath, Y.; Dincă, M.; Yachandra, V. K.; Nocera, D. G. *J. Am. Chem. Soc.* **2010**, *132*, 13692.

(12) (a) Surendranath, Y.; Kanan, M. W.; Nocera, D. G. *J. Am. Chem. Soc.* **2010**, *132*, 16501−16509. (b) Each Co occupies a cube 5 Å in width; defining a volume of 125 $Å^3$. Each monolayer contains 6.64 $10^{-10}$ mol of Co/$cm^2$ (note that there is a mistake in the numerical evaluation

of film thickness in ref 12a in which one monolayer is estimated to correspond to 1.65 $10^{-9}$ mol of Co/cm$^2$)

(13) (a) Esswein, A. J.; Surendranath, Y.; Reece, S. Y.; Nocera, D. G. *Energy Environ. Sci.* **2011**, *4*, 499. (b) Farrow, C. L.; Bediako, D. K.; Surendranath, Y.; Nocera, D. G.; Billinge, S. J. L. *J. Am. Chem. Soc.* **2013**, *135*, 6403.

(14) (a) Tafel, J.; Hahl, H. 1907, *40*, 3312. (b) Tafel equation is a large overpotential version (where the reaction is irreversible) of the more general Butler–Volmer relationship between current and potential for an electrochemical reaction, which spans the whole range of overpotentials (ref 14c,d). (c) Erdey-Grúz, T.; Volmer, M. *Z. Phys. Chem. (A)* **1930**, *150*, 203. (d) Butler, J. A. V. *Trans. Faraday Society* **1924**, *19*, 729.

(15) Biczok, L.; Linschitz, H. *J. Phys. Chem.* **1995**, *99*, 1843.

(16) Blauch, D. N.; Savéant, J.-M. *J. Am. Chem. Soc.* **1992**, *114*, 3323.

(17) Savéant, J.-M. *J. Electroanal. Chem.* **1991**, *302*, 91.

(18) It may alternatively be expressed in terms of $E^0_{Q+ZH/PH+Z}$ by application of eq 4:

$$\log I_0 = \log\left[\frac{C^0_Z}{C^0_{ZH}}\sqrt{I_k I_{H,e}}\tanh\left(\sqrt{\frac{I_k}{I_{H,e}}}\right)\right] + \frac{F(E^{eq}_A - E^0_{Q+ZH/PH+Z})}{RT\ln 10}$$

$$= \log\left[F\frac{C^0_Z}{C^0_{ZH}}C_{cat}k_{cat}d_f^{opt}\tanh\left(\frac{d_f}{d_f^{opt}}\right)\right] + \frac{F(E^{eq}_A - E^0_{Q+ZH/PH+Z})}{RT\ln 10} \quad (7')$$

(19) or, alternatively by

$$I_0^{max} = F\frac{C^0_Z}{C^0_{ZH}}C_{cat}\sqrt{k_{cat}D_{H,e}}\exp\left[\frac{F(E^{eq}_A - E^0_{Q+ZH/PH+Z})}{RT}\right]$$

$$= F\frac{C^0_Z}{C^0_{ZH}}C_{cat}k_{cat}d_f^{opt}\exp\left[\frac{F(E^{eq}_A - E^0_{Q+ZH/PH+Z})}{RT}\right] \quad (9')$$

(20) For the notion of "pure kinetic conditions" see ref 7c, p. 82.

(21) Bard, A. J.; Faulkner, L. R. *Electrochemical Methods: Fundamentals and Applications*, 2nd ed; John Wiley and Sons: New York, 2001; Chapter 9.

(22) *Standard Potentials in Aqueous Solutions*; Bard, A. J., Jordan, J., Parsons, R., Eds.; Marcel Dekker: New York, 1985.

(23) *Handbook of Chemistry and Physics*, 81st ed.; Lide, D. R., Ed.; CRC Press: Boca Raton, FL, 2000–2001; pp 5–95.

(24) Above pH = 7, $OH^-$ start to interfere as an additional CPET proton acceptor. The reactions that have $OH^-$ and other species as proton acceptor are under current investigation.

(25) (a) A similar behavior is observed with Ni–$B_i$ films in unbuffered pH 8.5 electrolyte where the slopes of the KL plots change (see Figure S6 in ref 25b) suggesting that in the later case the limiting factor is diffusion of $OH^-$ which is the acting base in the PCET processes. This ultimately leads to current density that plateaus (see Figure 7 in ref 25b). (b) Bediako, D. K.; Surendranath, Y.; Nocera, D. G. *J. Am. Chem. Soc.* **2013**, *135*, 3662.

(26) *Handbook of Chemistry and Physics*, 81st ed.; Lide, D. R., Ed.; CRC Press: Boca Raton, FL, 2000–2001; pp 5–96.

(27) (a) Costentin, C.; Drouet, S.; Robert, M.; Savéant, J.-M. *J. Am. Chem. Soc.* **2012**, *134*, 11235. (b) Costentin, C.; Drouet, S.; Robert, M.; Savéant, J.-M. *Science* **2012**, *338*, 90. (c) The turnover frequency at zero overpotential introduced in refs 27a,b is in fact the analog of $k_{cat}\exp[(F/RT)(E^{eq}_A - E^0_{Q+ZH/PH+Z}$ or $E^0_{Q+H+/PH})]$, which implies that $C_{cat}$ in the film could have been estimated.

(28) Surendranath, Y.; Bediako, D. K.; Nocera, D. G. *Proc. Natl. Acad. Sci. U.S.A.* **2012**, *109*, 15617.